AWARD NUMBER:	W81XWH-19-1-0168
TITLE:	Quantitative Assessment of Post-Traumatic Osteoarthritis by Multimodal Optical Coherence Tomography
PRINCIPAL INVESTIGATOR:	B. Hyle Park
CONTRACTING ORGANIZATION:	The Regents of the University of California
REPORT DATE:	July 2022
TYPE OF REPORT:	Annual Technical Report
PREPARED FOR:	U.S. Army Medical Research and Development Command Fort Detrick, Maryland 21702-5012
DISTRIBUTION STATEMENT:	Approved for Public Release; Distribution Unlimited

REPORT DOCUMENTATION PAGE

Form Approved
OMB No. 0704-0188

1. REPORT DATE	2. REPORT TYPE	3. DATES COVERED
JULY 2022	Annual	06/01/2021-5/31/2022

4. TITLE AND SUBTITLE

Quantitative Assessment of Post-Traumatic Osteoarthritis by Multimodal Optical Coherence Tomography

5a. CONTRACT NUMBER
W81XWH-19-1-0168

5b. GRANT NUMBER

5c. PROGRAM ELEMENT NUMBER

6. AUTHOR(S)
B. Hyle Park, Jin Nam

E-Mail: hylepark@engr.ucr.edu; jnam@engr.ucr.edu

5d. PROJECT NUMBER

5e. TASK NUMBER

5f. WORK UNIT NUMBER

7. PERFORMING ORGANIZATION NAME(S) AND ADDRESS(ES)
California, University of, Riverside
200 University Office
Building
Riverside, CA 92521

8. PERFORMING ORGANIZATION REPORT NUMBER

9. SPONSORING / MONITORING AGENCY NAME(S) AND ADDRESS(ES)

U.S. Army Medical Research and Development Command
Fort Detrick, Maryland 21702-5012

10. SPONSOR/MONITOR'S ACRONYM(S)

11. SPONSOR/MONITOR'S REPORT NUMBER(S)

12. DISTRIBUTION / AVAILABILITY STATEMENT

Approved for Public Release; Distribution Unlimited

13. SUPPLEMENTARY NOTES

14. ABSTRACT
Evidence from osteoarthritis (OA) studies suggests that there is a narrow time window in the early stages of the disease when cartilage can be functionally restored to reduce further degeneration. Small internal cartilage damages due to traumatic joint injuries are hard to detect with the traditional imaging technologies but pose a significant risk of inducing OA later. Our goal is to develop a non-destructive and label-free combination of optical coherence tomography (OCT) based methods for early detection of PTOA by assessment of mechanical strength, which is dependent upon both GAG and collagen, through our novel method for optical coherence elastography (OCE) based on fringe washout, and of collagen by itself through polarization-sensitive OCT. While our progress has been slowed by the current COVID-19 pandemic, we have demonstrated, for the first time to our knowledge, volumetric assessment of the mechanical properties of cartilage and bone. We anticipate successful completion of our aims as our campus re-opens for research activities. This work will provide the first optical method capable of complete non-destructive assessment of sub-surface cartilage degeneration for PTOA diagnosis.

15. SUBJECT TERMS
post-traumatic osteoarthritis, early detection, cartilage, glycosaminoglycan, collagen, mechanical strength, Young's modulus, optical imaging, optical coherence tomography, optical coherence elastography, polarization-sensitive

16. SECURITY CLASSIFICATION OF:			17. LIMITATION OF ABSTRACT	18. NUMBER OF PAGES	19a. NAME OF RESPONSIBLE PERSON
a. REPORT	b. ABSTRACT	c. THIS PAGE			USAMRDC
Unclassified	Unclassified	Unclassified	Unclassified	12	19b. TELEPHONE NUMBER *(include area code)*

TABLE OF CONTENTS

1. INTRODUCTION

Evidence from osteoarthritis (OA) studies suggests that there is a narrow time window in the early stages of the disease when cartilage can be functionally restored to reduce further degeneration. These studies collectively demonstrate the importance of early detection of OA to enhance the effectiveness of subsequent therapies. However, current technologies, including arthroscopy, X-ray radiography, and MRI, can detect OA only after significant and irreversible damage to articular cartilage has already occurred. Small internal cartilage damages due to traumatic joint injuries are hard to detect with the traditional imaging technologies but pose a significant risk of inducing OA later. Therefore, it is essential to develop tomographic imaging tools with high resolution that can provide direct assessment of intra-cartilaginous damage in individual patients at the earliest stages of PTOA. We believe that high-resolution assessment of not only the surface, but also the interior portions of cartilage will allow for detection of OA at a much earlier time point, thus providing an opportunity to prevent the progression of or even to allow for repair of cartilage damage and to guide therapies to where they are most effective for existing damage. To take advantage of this therapeutic window, our goal is to develop a non-destructive and label- free combination of optical coherence tomography (OCT) based methods for early detection of PTOA. Cartilage damage at the early stages of OA is known to heterogeneously alter local density/mechanical properties of extracellular matrix (ECM). The mechanical properties of cartilage derive from extracellular matrix components of glycosaminoglycan (GAG) and collagen, with the density and organization of both known to change early in PTOA development. Several investigators have previously established PS-OCT as a method for quantifying localized changes in collagen, but this method is not sensitive to glycosaminoglycan (GAG), which also significantly contributes to the mechanical properties of cartilage. A smaller number of separate studies have investigated the use of optical coherence elastography (OCE) to examine the overall mechanical properties of cartilage, but these techniques cannot provide volumetric quantification in real time. Our novel method for OCE takes advantage of fringe washout, an artifact related to motion during the acquisition time of spectral domain OCT systems, and can be used to rapidly scan volumes of tissue in combination with PS-OCT. Our hypothesis is that robust and sensitive detection of early PTOA can be achieved by utilizing OCE to quantify subsurface damages in GAG loss and its associated cartilage swelling when complemented by quantification of localized changes in collagen content/disorganization with PS-OCT. This project has three aims: 1. optimize fringe washout based OCE, 2. optically quantify GAG in cartilage, and 3. identify optical signatures of cartilage degeneration in early stages of a rat PTOA model. Completion of these aims will provide the first optical method capable of complete non-destructive assessment of sub-surface cartilage degeneration for PTOA diagnosis.

2. KEYWORDS

post-traumatic osteoarthritis, early detection, cartilage, glycosaminoglycan, collagen
mechanical strength, Young's modulus
optical imaging, optical coherence tomography, optical coherence elastography, polarization-sensitive

3. ACCOMPLISHMENTS

What were the major goals of the project?

Specific Aim 1: optimize fringe washout based optical coherence elastography

- Major task 1: relative delay optimization
  - Milestone: autocalibration of optimized PS-OCT/OCT imaging system (month 4)
    - Progress: *110% (previously 100%) (improvements made to imaging protocol)*
- Major task 2: characterization of sensitivity and resolution
  - Milestone: optimized OCE acquisition parameters based on imaging scenario with expected sensitivity and resolution based on sample size and composition (month 7)
    - Progress: *120% (previously 100%) (significant technological improvements)*

Specific Aim 2: optically quantify GAG in cartilage

- Major task 1: bovine cartilage explant experimentation and analysis

- Milestone: calibrated determination of mechanical and biochemical properties of cartilage based on optical imaging (month 10)
  - Progress: 90% (previously 50%)

Specific Aim 3: identify optical signatures of cartilage degeneration in early stages of a rat PTOA model

- Major task 1: early rat OA model experimentation and analysis
  - Milestone: obtain ACURO approval, obtain UCR IACUC approval of protocol amendment (month 5)
    - Progress: *100% (previously 100%) (renewal of protocol submitted and approved by UCR IACUC)*
  - Milestone: identification of early PTOA based on optical assessment of changes in cartilage (month 18)
    - Progress: 90% (previously 50%)

What was accomplished under these goals?

Imaging protocol improvement – PS-OCT

In this reporting period, we improved our PS-OCT image processing pipeline to reduce the effect of speckle which will enable us to localize and quantify any changes in cartilage due to PTOA in terms of both the minimum size and degree of change required for detection.

As an interferometric technique based on coherent light, OCT images suffer from speckle which greatly obscure the structural details of biological tissues[1]. The presence of speckle becomes much more problematic for PS-OCT, especially when measuring changes in phase retardation within a small region or near the top surface of the tissues. In these regions, the variability due to speckle noise, often times 3-5-fold higher than shot-noise limited variability[2], overshadows the small changes in phase retardation. To resolve the substructural detail and reliably measure the change in phase retardation, we have adopted a multi-volume averaging approach. Since speckle pattern decorrelate with time, we acquire multiple volumes of data longitudinally from the same sample region. Averaging these multiple volumes greatly reduces the effect of speckle which is evident from our preliminary study done with mouse spinal cord. The mouse spinal cord has distinctive low birefringent gray matter region (dorsal horn) and highly birefringent white matter regions (dorsal, ventral and lateral funiculi). If we visually compare the cross-sectional intensity image Figure 1(b) with the multi-volume averaged image Figure 1(d), we notice that the border of the dorsal horn region is more prominent in the averaged image. Comparison between the cross-sectional depth-resolved phase retardation image Figure 1(c) and its multi-volume average image Figure 1(e) shows that the highly birefringent white matter regions (represented by warmer colors) can be delineated more accurately from the averaged image. Also, small local

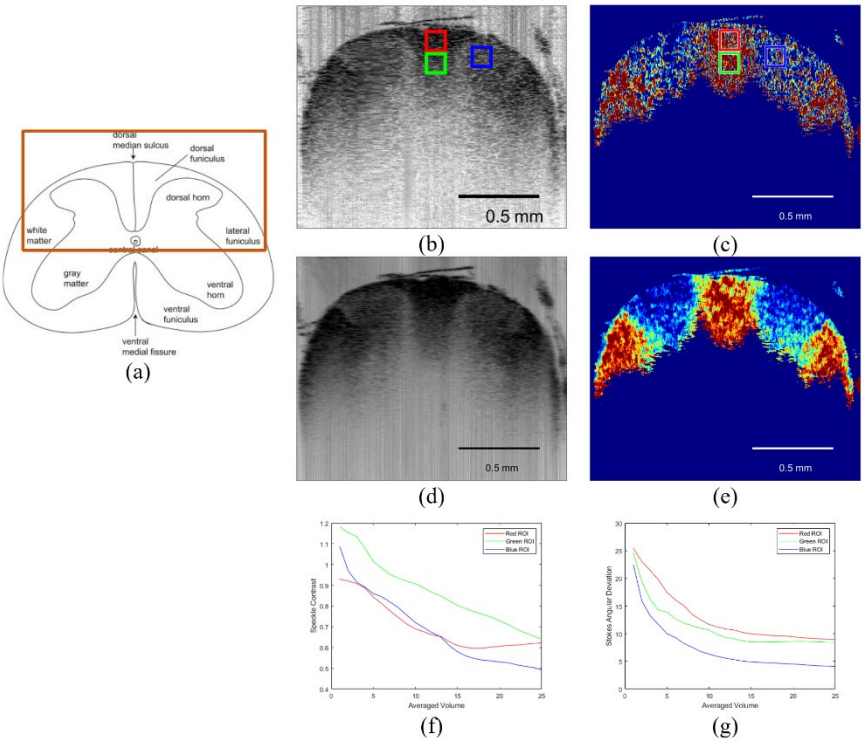

Figure 1: (a) General anatomy of mouse spinal cord. The box highlights the region that can be seen in the cross-sectional images (b)-(e). (b) and (d) shows the intensity images while (c) and (e) shows the depth-resolved phase retardation images. (b) and (c) show cross-section from a single volume while (d) and (e) are the same cross-sectional images obtained after averaging longitudinally acquired 25 volumes. Visual comparison clearly shows improved structural details and clearly identifiable local changes in phase retardation in the averaged images. (f) and (g) measures the reduction in speckle noise achieved with averaging the intensity and the phase-retardation images, respectively, in the regions highlighted in (b) and (c). The improvement in the intensity image, measured with speckle contrast, is 2 fold while the improvement in the phase-retardation image, measured with Stokes angular deviation, is almost 5 fold.

[1] J. M. Schmitt, S. H. Xiang, and K. M. Yung, "Speckle in Optical Coherence Tomography," J. Biomed. Opt., vol. 4, no. 1, p. 95, 1999, doi: 10.1117/1.429925.

[2] E. Götzinger et al., "Speckle noise reduction in high speed polarization sensitive spectral domain optical coherence tomography," Opt. Express, vol. 19, no. 15, p. 14568, Jul. 2011, doi: 10.1364/OE.19.014568.

changes in phase retardation can be easily identified in Figure 1(e) which are completely obscured by the speckle granules in Figure 1(c). The reduction in speckle noise in the intensity image is measured with speckle contrast and is shown in Figure 1(f). We can see that the speckle contrast has reduced almost 2 folds in different regions highlighted by the boxes in Figure 1(b). The reduction in speckle noise in the phase retardation image is measured with Stokes angular deviation which achieves almost 5 fold reduction as shown in Figure 1(g).

Based on these preliminary results, we are confident that by using multi-volume averaging method to reduce the effects of speckle, we will be better able to localize and quantify small changes in birefringence after re-imaging our bovine and rat cartilage PTOA samples.

System development – OCE

A number of minor artifacts along with an observed need to insure robustness of the hardware required to implement our method for OCE were observed through a careful examination of our data during the last reporting period. In brief, we had several ultrasound transducers of different varieties burn out, which prompted investigation into possible reasons for the problems as well as exploration of different transducer types and geometries. This latter point was also motivated by the discovery of regions in which there was little to no ultrasound-induced perturbation of tissue, resulting in an inability to determine the Young's modulus within these regions. Our work during the reporting period is described in greater detail in the following paragraphs.

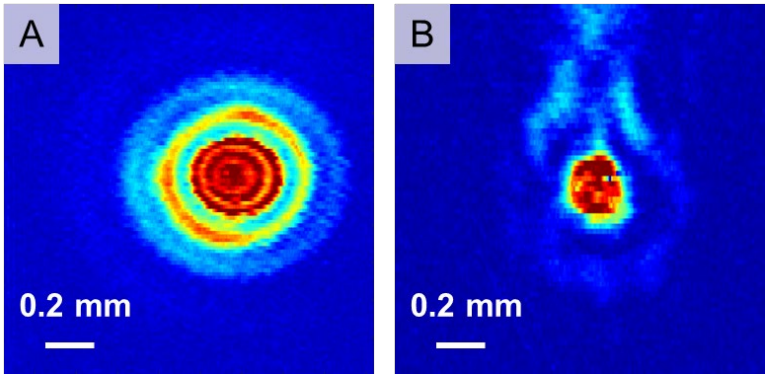

Figure 2: Example en face OCE images constructed from data taken with ultrasound excitation from the initially-used 6.8 MHz point focus transducer. A) En face OCE image of a homogeneous elastic phantom. The concentric ring pattern is likely caused by acoustic diffraction at the ultrasound focus. B) En face OCE image of in vitro rat femur cartilage. The image artifact may be caused by combined effects from acoustic diffraction and interference from uncontrolled reflected ultrasound. (All OCE images are in jet colormap, where the red represents high OCE values and blue represents low OCE values)

Our fringe washout OCE method is based on the examination of the differences in signal intensity between depth profiles acquired with and without ultrasound excitation in consecutive OCT scans. Fringe washout effect presents in the depth profiles acquired with sample vibration in response to ultrasound perturbation, resulting in an OCT imaging artifact in which the sample signal-to-noise ratio (SNR) decreases. The magnitude of localized vibration, dependent on the mechanical stiffness of the sample, can be estimated by quantifying the amount of fringe washout SNR decrease, and OCE data can be obtained by simply subtracting the SNR of depth profiles with ultrasound from that of depth profiles without ultrasound at corresponding locations. This method is computationally efficient, and does not require repeated scanning at one lateral position and strict imaging conditions (e.g. phase stability) as most OCE techniques do, making it possible to implement real-time volumetric visualization of OCE data across a certain area on the sample. Given that our method to assess sample stiffness is solely based on the measurement of local displacement, to achieve this goal, a wide and uniform ultrasound field is preferred to ensure the ultrasonic stress within the field-of-view (FOV) is equal.

In the last progress report, we summarized OCE data obtained with a customized 6.8 MHz point focus transducer with a concentric round hole in the center to allow OCT beam to travel through to reach the sample. However, the lateral size of the ultrasound focal spot is only about 0.3 mm in full width at half maximum (FWHM) diameter, which is much smaller than the image FOV (several mm), and the ultrasound pressure applied on the cartilage surface is not uniform. This nature of the point focus transducer makes it difficult to achieve an en face OCE map that represents the distribution of stiffness of the cartilage surface. In addition, we observed different image artifacts (example shown in Figure 2) caused by acoustic diffraction pattern near the transducer focus and/or the interference pattern induced by reflected acoustic waves. To overcome these intrinsic limitations of the point focus transducer, over the past year, we have investigated other types of transducers and developed a fringe washout-based method, similar to our OCE method, to characterize the ultrasound magnitude field.

To obtain a uniform ultrasound field and reduce the acoustic diffraction effect at ultrasound focus, we initially applied a 1 MHz non-focused flat transducer. The ultrasound field reaches its optimal uniformity at approximately 200 mm from the transducer piezo surface, so we modified the OCE imaging configuration in which the ultrasound waves are transmitted from the side of the sample and the OCT beam scans from the top (as shown in Figure 3a and b). Figure 3c and d show the cross-sectional and reconstructed en face OCE images of a 6.25 mm by 6.25 mm lateral region on elastic phantom and cartilage samples, respectively, under the ultrasound excitation from the flat transducer. The size of ultrasound perturbed area is large enough to cover the whole FOV, however, we noticed a banding pattern artifact on both cross-sectional and en face views which degraded the uniformity of the ultrasound field and might potentially obscure the local differences in sample mechanical properties represented by OCE values. Further analysis and tests revealed that the banding pattern artifact was caused by acoustic standing waves from the interference between the incident waves and returning waves reflected on acoustic barriers, such as the wall of the water tub or the sample holding fixture (Figure 3). The banding pattern artifact can be removed by extending the distance between the sample and the barrier, or applying shorter duration of ultrasound pulses, but these solutions brought new challenges of experiment space requirements or insufficient acoustic excitation power.

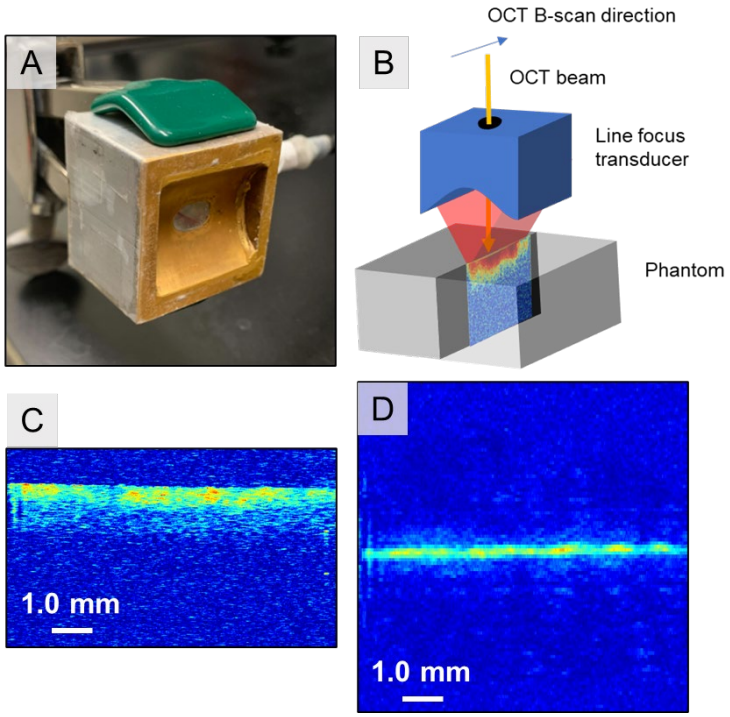

Figure 3: Application of the customized 3 MHz line focus transducer for OCE imaging. A) A picture of the semi-cyindrical line focus transducer. B) A diagram that shows the transducer and phantom setup to acquire OCT data. C) Cross-sectional OCE image of a homogeneous elastic phantom in the center of the focus line. It can be noticed that the ultrasound field is uniform in the lateral direction across a frame of B-scan (no banding artifact). However, the pressure field is not evenly distributed versus depth. D) En face OCE image of the elastic phantom. The focus line (~ 0.5 mm wide) can be clearly seen in the middle and the ultrasound intensity distribution is uniform.

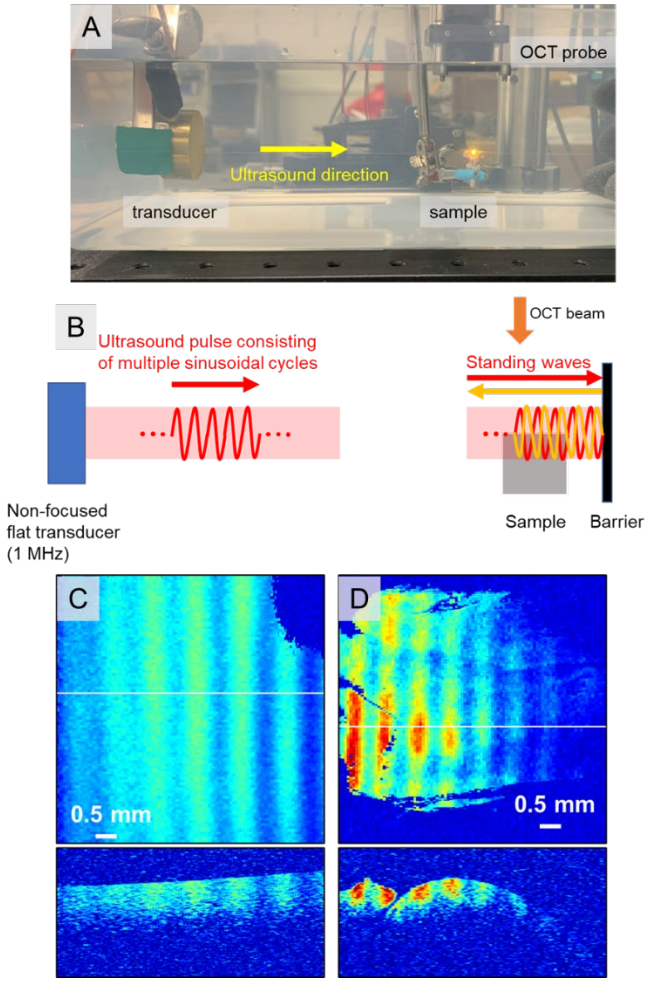

Figure 4: Experiment setup with the 1 MHz non-focus flat transducer and example en face OCE image with banding artifacts. A) the experiment setup, with the transducer placed about 200 mm to the side of the sample. The OCT probe is above the sample and scans from the top. B) A diagram that shows the cause of the banding pattern on the OCE images. One pulse of ultrasound, consisting of a train of multiple cycles of ultrasound waves, is transmitted from the transducer and propagates through water and the sample until being reflected by an acoustic barrier (e.g. the water tub wall). The returning waves interfere with the remaining incident waves (or the next pulse in some cases), creating a standing wave on the sample. C) and D) OCE en face and cross-sectional images of an elastic phantom (C) and rat femur cartilage (D) with standing wave-caused banding artifacts. The thin white lines on en face images indicate the lateral position of the example cross-sectional images.

We then employed a customized 3 MHz line focus transducer and hoped to avoid standing wave artifacts as well as to obtain a laterally uniform ultrasound field along the direction of one OCT B-scan. As shown in Figure 4a, the shape of the piezo surface of the transducer is cylindrical, capable of focusing the ultrasound waves on the axis to form a 0.5 mm wide line field ultrasound

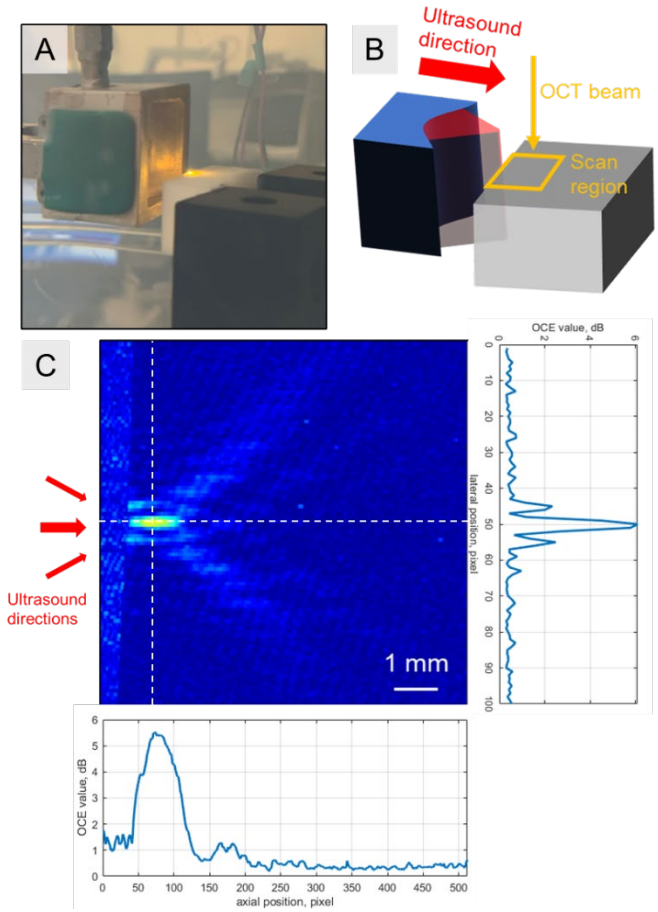

Figure 5: Setup and result of fringe washout-based ultrasound field characterization. A) and B) A picture and a diagram of the transducer setup to characterize the ultrasound field of the line focus transducer. OCT scans from the top and FOV is set to cover the ultrasound focus near the edge of the sample. An en face OCE image is generated to visualize the ultrasound field in the post-processing. C) Reconstructed en face OCE image that shows the ultrasound pressure distribution. The graphs on the right and bottom sides of the en face OCE image plot the ultrasound intensity, represented by OCE values, versus lateral location as indicated by the vertical and horizontal dashed white lines, respectively.

the ultrasound pressure can be assessed based on the OCE data of a homogeneous elastic phantom. Given that OCT only allows to see features within the depth of about 1.5 mm, the ultrasound behavior beyond the OCT depth range is hidden with the same co-focus setup as shown in Figure 4c. To extend the visualization range along the ultrasound axial direction, we designed a new setup where we placed the transducer on the side of the phantom and scanned the phantom from the top (Figure 5a and b). In this configuration, the propagation direction of the ultrasound is perpendicular to OCT A-scans and thus the visualization of the ultrasound field is not limited by the OCT penetration depth. A complete ultrasound pressure distribution map can be generated with en face view reconstruction from the volumetric data. Figure 5c shows the ultrasound field characterization result within a 8 focus. There is a hole in the middle of the piezo surface to allow the OCT beam to pass through. Before acquiring OCE data, the transducer is aligned carefully to ensure the ultrasound is axially focused on the same depth as the optical focus, and the orientation of the ultrasound focus line is well-aligned with the OCT B-scan direction (Figure 4b). With the same OCE data acquisition scheme, we were able to obtain volumetric OCE data of a homogeneous elastic phantom. Figure 4c shows a cross-sectional view of the frame of B-scan along the ultrasound line focus. The ultrasound pressure across the lateral span of FOV is uniform. The complete lateral distribution of the ultrasound field can be visualized on the en face reconstruction of volumetric data (Figure 4d), on which the center line represents the highly excited region at ultrasound focus. The line focus transducer can avoid the occurrence of standing wave pattern and along the longitudinal direction of the focus line, it has significantly reduced the focusing diffraction artifact.

Due to the focusing nature of ultrasound, the acoustic pressure distribution in the axial direction is not uniform and acoustic diffraction effect near the focus also alters the stress applied on the sample. To achieve a reliable OCE map of sample stiffness, it is important to know the distribution of stress applied on the sample. We hoped to estimate the relative stress level by characterizing the distribution of the ultrasound pressure field and use it to correct the raw OCE data. Our OCE method measures the magnitude of local displacement under the assumption of an evenly distributed stress field to determine the local mechanical properties of the sample; if the sample is known to be mechanically homogeneous, the measured OCE value should represent the variation in the stress applied. Therefore,

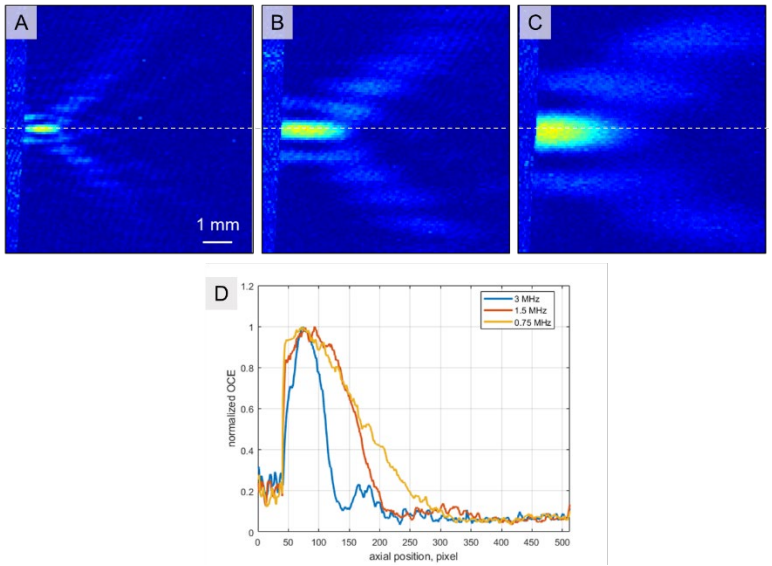

Figure 6: Ultrasound field characterization results of different sizes of focus area by adjusting the driving frequencies to integer halves of the resonant frequency. The size of the focus area gets larger at lower frequencies and the side lobes become farther apart. A), B) and C) show the ultrasound intensity field at 3 MHz (resonant frequency), 1.5 MHz and 0.75 MHz. D) shows the normalized ultrasound intensity profile along axial direction at and beyond the focal area.

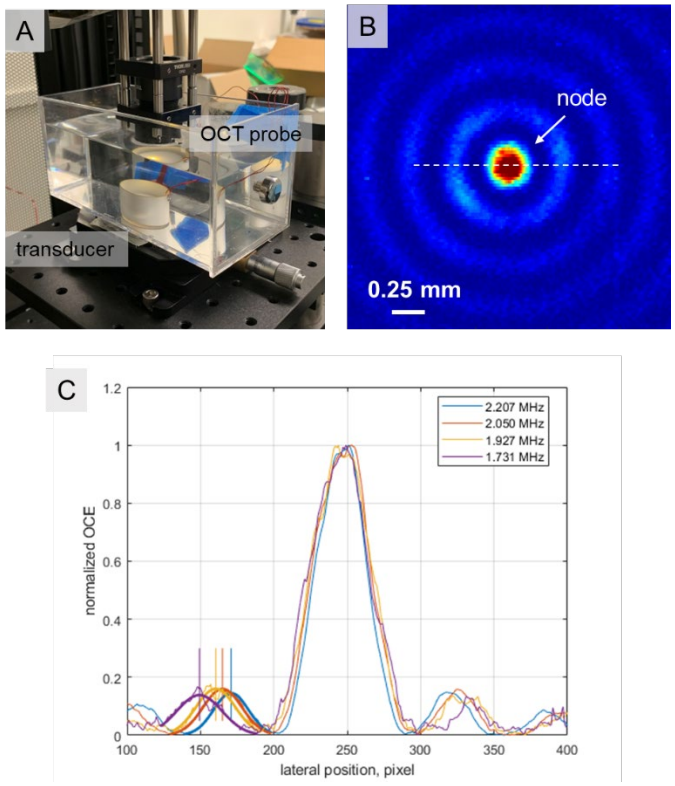

Figure 7: Characterization of the 2.207 MHz cylindrical tube piezo transducer. A) A picture of the setup of the tube transducer to characterize its ultrasound field. The transducer is placed on the bottom of the water tube and a piece of PDMS phantom is placed inside of the piezo tube. OCT probe scans from the top of the phantom. B) Measured ultrasound pressure distribution map. Concentric ring patterns can be seen due to the standing wave effect. C) The ultrasound intensity profiles vs lateral position as indicated by the white dash line in B). The relative ultrasound intensity is represented by normalized OCE values. The center of the first lobe is determined and marked with a short vertical line. On the graph, ultrasound intensity profiles at different frequencies are compared. At lower frequencies, the position of the first side lobe gets farther from the center ultrasound-excited region and the radius of the first ring is greater.

mm by 8 mm scan region. The region with maximum OCE values represents the ultrasound focus and the axial ultrasound intensity profile exhibits an approximate Gaussian distribution. With these ultrasound characterization results, the error on the OCE measurement caused by the position-dependent variation of stress applied on the sample can be corrected.

On the other hand, the size of the ultrasound focal region is determined by the geometry of the piezoelectric crystal and the ultrasound frequency. Driven at its resonant frequency, the transducer will operate most efficiently and deliver the maximal power output; however, at lower frequencies, the size of the focal region will be larger according to ultrasound focusing properties. This feature provides us with another direction to achieve a larger and more uniform ultrasound field: lower the ultrasound frequency. Figure 6 shows the ultrasound field under 3 MHz (resonant frequency), 1.5 MHz and 0.75 MHz. As the ultrasound frequency gets lower, the size of the ultrasound focus increases in both axial and lateral directions. The side lobes caused by wave interference also gets farther apart. Operating at lower frequencies makes the ultrasound pressure more uniformly distributed and reduces the chance of the occurrence of fixed pattern artifacts on the OCE images.

One common disadvantage of the three types of transducers is that their ultrasound field is open to the surrounding environment and can be distorted by nearby objects (such as sample holding fixtures). In addition, the open ultrasound field is sensitive to the positioning of the transducer, which makes it difficult to be aligned with the OCT scan beam practically. A cylindrical tube transducer (Figure 6 a) is capable of generating a closed and predictable ultrasound field without the interference from the outside. Herein, we also tested a piezo tube transducer (Physik Instrumente, Karlsruhe, Germany) with an experiment-determined resonant frequency of 2.207 MHz. With the same acoustic pressure field characterization method, the ultrasound distribution in the center of the tube shows concentric rings pattern due to the standing wave effect (Figure 7b). The position and width of the node regions, where the ultrasound waves get deconstructed between two highly ultrasonic-excited “rings”, can be manipulated by altering the ultrasound frequency. Figure 7c compares the ultrasound pressure profiles, represented by normalized OCE values, under different driving frequencies. The radius of the first ring, shown as the position of the center of the first lobe on the profile, can be enlarged by applying a lower frequency. This feature allows to expand the ultrasound-affected area by varying the ultrasound frequency and an equivalent large and stable ultrasound field can be obtained by combining the ultrasound distribution taken at different frequencies. The OCE data acquired at corresponding frequencies can be corrected and combined based on the ultrasound field characterization to achieve a map of cartilage stiffness distribution.

One of the most important results of the improvements to OCE over the reporting period is that the cylindrical transducers will allow for simultaneous acquisition of PS-OCT and OCE data. We will re-image all samples generated over the course of this project to dissect out the separate contributions of GAG and collagen over the course of PTOA induction.

What opportunities for training and professional development has the project provided?

Nothing to report.

How were the results disseminated to communities of interest?
Nothing to report.

What do you plan to do during the next reporting period to accomplish the goals?
COVID-19 has continued to periodically result in unexpected delays on this overall project, including with submission of this report. We have only a limited number of activities remaining to complete the proposed work, largely encompassed by utilizing the improved methodology for both PS-OCT and OCE, as well as simultaneous (as opposed to sequential) acquisition of imaging data on the bovine and rat samples.

4. IMPACT

What was the impact on the development of the principal discipline(s) of the project?
We anticipate that, upon completion of analysis of these results, we will be able to provide the first demonstration, to the best of our knowledge, of the ability to non-destructively assess loss of collagen structure and of GAG structure in cartilage in PTOA. We expect to achieve this based on our preliminary results that at this point confirm that OCE can detect changes in mechanical strength due to a loss of both collagen and GAG structure, and that PS-OCT largely quantifies loss of collagen. The impact of our current progress opens the possibility of non-destructive assessment of volumetric mechanical properties of cartilage as a method for early detection of PTOA onset and progression.

What was the impact on other disciplines?
Nothing to report.

What was the impact of technology transfer?
Nothing to report.

What was the impact on society beyond science and technology?
Nothing to report.

5. CHANGES / PROBLEMS

Changes in approach and reasons for change
No changes to report.

Actual or anticipated problems or delays and actions or plans to resolve them
Periodic delays have been encountered as different research participants have been sidelined by COVID. We have decided that the most effective overall approach is to assume that unexpected absences or delays might come at any time, and so have been trying to make sure that at least some overlap of effort on any given aspect of the project to try to maintain progress in the event of a COVID-related absence or delay. This has, on occasion, still resulted in delays as there have been at least two occasions over the past year when all participants on a particular aspect of the project have been in simultaneous self-quarantine but this has been a reasonably effective solution.

Changes that had a significant impact on expenditures
No changes to report.

Significant changes in use or care of human subjects

N/A.

Significant changes in use or care of vertebrate animals
No changes to report.

Significant changes in use or biohazards and/or select agents
N/A.

6. PRODUCTS

Nothing to report.

7. PARTICIPANTS & OTHER COLLABORATING ORGANIZATIONS

What individuals have worked on the project?

Name:	B. Hyle Park
Project Role:	PI
Research Identifier:	https://orcid.org/0000-0002-0282-7162
Nearest person month worked:	3
Contribution to project:	Supervision of overall project progress through weekly meetings

Name:	Jin Nam
Project Role:	PI
Research Identifier:	https://orcid.org/0000-0001-5117-8958
Nearest person month worked:	3
Contribution to project:	Supervision of overall project progress through weekly meetings

Name:	Junze Liu
Project Role:	Graduate student
Research Identifier:	https://orcid.org/0000-0001-7946-4833
Nearest person month worked:	12
Contribution to project:	Design and construction of OCE system; optimization of processing method to visualize tissue mechanical properties

Name:	Youyi Tai
Project Role:	Graduate student
Research Identifier:	https://orcid.org/0000-0002-2530-4225
Nearest person month worked:	12
Contribution to project:	Preparation of bovine explant samples, perform drop tower injuries, preparation of animal models

Name:	Thamidul Islam
Project Role:	Graduate student
Research Identifier:	https://orcid.org/0000-0002-8430-1104
Nearest person month worked:	9
Contribution to project:	Polarization-sensitive OCT data acquisition and analysis

Name:	Luyang Yu
Project Role:	Graduate student
Research Identifier:	
Nearest person month worked:	3

Contribution to project:	OCE data acquisition and analysis

Has there been a change in the active other support of the PD/PI(s) or senior/key personnel since the last reporting period?
There have been no changes to the active other support for the PD/PI(s).

What other organizations were involved as partners?
Nothing to report.

8. SPECIAL REPORTING REQUIREMENTS

N/A.

9. APPENDICES

N/A.